INTERNATIONAL JOURNAL FOR NUMERICAL METHODS IN FLUIDS, VOL. 22, 429–444 (1996)

ON BREAKING WAVES AND WAVE–CURRENT INTERACTION IN SHALLOW WATER: A 2D*H* FINITE ELEMENT MODEL

J. S. ANTUNES DO CARMO AND F. J. SEABRA-SANTOS

IMAR, Faculdade de Ciências e Tecnologia, Universidade de Coimbra, 3049 Coimbra Codex, Portugal

SUMMARY

A two-dimensional (horizontal plane) coastal and estuarine region model, capable of predicting the combined effects of gravity surface shallow-water waves (shoaling, refraction, diffraction, reflection and breaking), and steady currents, is described and numerical results are compared with those obtained experimentally.

Two series of observations within a wave flume and a combined wave-current facility were developed. In the first case, the wave was generated via a hinged paddle located within a deepened section at one end of the channel, as, in the second case, the wave propagating with or against the current was generated by a plunger-type wavemaker; the re-circulating current was introduced via one passing tank connected to a centrifugal pump.

Several comparisons for a number of 1*D* situations and one 2*D* horizontal plane case are presented.

KEY WORDS: modified Boussinesq equations; finite element method; wave-current interaction; breaking waves

1. INTRODUCTION

Coastal and estuarine region flows are strongly influenced by, among other phenomena like refraction, diffraction, reflection, etc., complex superposition of non-linear wave–wave and wave–current interactions. So, as is widely recognised in the literature,[4–8] the use of a classical wave model that does not take into account wave–current interactions, is considered to be somewhat incomplete. Other effects must be also considered, such as those resulting from bottom friction and eventually from the wave breaking, the latter being also responsible for producing littoral currents.

The purpose of this paper is to present an original finite element technique improvement to the classical 2*D* (horizontal plane) shallow-water wave models based on the *Boussinesq* equations to introduce the breaking effects and interactions between waves and steady currents.

At a distance from the surf zone, where the effects of wave breaking are non-existent, the current characteristics are relatively well known, or they can be, either through *in situ* measurement, or a large zone modelling of the ocean circulation. Then, a regional or local model based on a more detailed geometry and bathymetry is able to provide the current velocity field installed, at a given moment, in the coastal region under study.

The hydrodynamic model presented here, can be used to study the wave propagation and breaking over this steady current velocity field. There is no practical limitation for the definition of current velocity, as it may be less than, equal to or greater than the wave orbital velocity.

2. FORMULATION

The modified Boussinesq-type equations presented in this paper are deduced from the fundamental fluid mechanics equations relating to a three-dimensional and quasi-irrotational flow of a viscous and incompressible fluid, written in Euler's variables.

CCC 0271–2091/96/050429–16

Received July 1994
Revised March 1995

Considering the characteristic quantities a, H and l, which represent wave amplitude, mean water depth and a characteristic length, respectively, the following nondimensional variables can be defined:

$$x^* = x/l, \quad y^* = y/l, \quad z^* = z/H, \quad \eta^* = \eta/a, \quad \xi^* = \xi l^2/H^3,$$
$$u^* = \frac{u}{a\sqrt{(g/H)}} = \frac{uH}{ac_0}; \quad v^* = \frac{v}{a\sqrt{(g/H)}} = \frac{vH}{ac_0}, \quad w^* = \frac{wl}{aH\sqrt{(g/H)}} = \frac{wl}{ac_0},$$
$$u_c^* = \frac{u_c l}{Hc_0}, \quad v_c^* = \frac{v_c l}{Hc_0}, \quad t^* = \frac{\sqrt{(gH)}t}{l} = \frac{c_0 t}{l}, \quad P^* = \frac{P}{\rho g H},$$
$$\tau_{xx}^* = \frac{\tau_{xx}}{gH}, \quad \tau_{xy}^* = \frac{\tau_{xy}}{gH}, \quad \tau_{xz}^* = \frac{\tau_{xz}}{gH}, \quad \tau_{yy}^* = \frac{\tau_{yy}}{gH}, \quad \tau_{yz}^* = \frac{\tau_{yz}}{gH}, \quad \tau_{zz}^* = \frac{\tau_{zz}}{gH},$$

where $c_0 = \sqrt{(gH)}$, t is the time, η is the surface elevation, ξ represents the bathymetry; u, v, w, u_c and v_c are velocity components (the subscript c denotes current), P is the pressure, ρ is the specific mass of the fluid, g is the gravitational acceleration, and τ_{xx}, τ_{xy}, τ_{yy}, τ_{xz} and τ_{zz} are stress tensor components. The asterisk is used to denote non-dimensional variables.

We have chosen a co-ordinate system where Ox and Oy coincide with the free-surface at rest and Oz is positive upward.

Defining the small non-dimensional quantities $\epsilon = a/H$ and $\sigma = H/l$, which are measures of nonlinearity and frequency dispersion, respectively, the new variables U^* and V^* may be defined:

$$U^* = \frac{u + u_c}{\epsilon c_0} = u^* + \frac{\sigma}{\epsilon} u_c^*,$$

$$V^* = \frac{v + v_c}{\epsilon c_0} = v^* + \frac{\sigma}{\epsilon} v_c^*.$$

Accordingly, the fundamental equations for the fluid motion, the vorticity components and the usual kinematic and dynamic boundary conditions are written as follows:

Fundamental equations

$$\frac{\partial U^*}{\partial x^*} + \frac{\partial V^*}{\partial y^*} + \frac{\partial W^*}{\partial z^*} = 0, \tag{1}$$

$$\epsilon\sigma \frac{\partial U^*}{\partial t^*} + \epsilon^2 \sigma U^* \frac{\partial U^*}{\partial x^*} + \epsilon^2 \sigma V^* \frac{\partial U^*}{\partial y^*} + \epsilon^2 \sigma W^* \frac{\partial U^*}{\partial z^*}$$
$$= -\sigma \frac{\partial P^*}{\partial x^*} + \sigma \frac{\partial \tau_{xx}^*}{\partial x^*} + \sigma \frac{\partial \tau_{xy}^*}{\partial y^*} + \frac{\partial \tau_{xz}^*}{\partial z^*}, \tag{2}$$

$$\epsilon\sigma \frac{\partial V^*}{\partial t^*} + \epsilon^2 \sigma U^* \frac{\partial V^*}{\partial x^*} + \epsilon^2 \sigma V^* \frac{\partial V^*}{\partial y^*} + \epsilon^2 \sigma W^* \frac{\partial V^*}{\partial z^*}$$
$$= -\sigma \frac{\partial P^*}{\partial y^*} + \sigma \frac{\partial \tau_{yx}^*}{\partial x^*} + \sigma \frac{\partial \tau_{yy}^*}{\partial y^*} + \frac{\partial \tau_{yz}^*}{\partial z^*}, \tag{3}$$

$$\epsilon\sigma^2 \frac{\partial W^*}{\partial t^*} + \epsilon^2 \sigma^2 U^* \frac{\partial W^*}{\partial x^*} + \epsilon^2 \sigma^2 V^* \frac{\partial W^*}{\partial y^*} + \epsilon^2 \sigma^2 W^* \frac{\partial W^*}{\partial z^*}$$
$$= -\frac{\partial P^*}{\partial z^*} + \sigma \frac{\partial \tau_{zx}^*}{\partial x^*} + \sigma \frac{\partial \tau_{zy}^*}{\partial y^*} + \frac{\partial \tau_{zz}^*}{\partial z^*} - 1, \tag{4}$$

Vorticity components

$$\Omega_x^* = \sigma^2 \frac{\partial W^*}{\partial y^*} - \frac{\partial V^*}{\partial z^*}, \quad \Omega_y^* = \frac{\partial U^*}{\partial z^*} - \sigma^2 \frac{\partial W^*}{\partial x^*},$$
$$\Omega_z{}^* = \frac{\partial V^*}{\partial x^*} - \frac{\partial U^*}{\partial y^*}, \tag{5}$$

Boundary conditions

At the *free surface*, $z^* = \epsilon\eta^*(x^*, y^*, t^*)$

$$\frac{\partial \eta^*}{\partial t^*} + \epsilon U^* \frac{\partial \eta^*}{\partial x^*} + \epsilon V^* \frac{\partial \eta^*}{\partial y^*} = W^*, \tag{6}$$

$$-\epsilon\sigma\tau_{xx}^* \frac{\partial \eta^*}{\partial x^*} - \epsilon\sigma\tau_{xy}^* \frac{\partial \eta^*}{\partial y^*} + \tau_{xz}^* = \tau_{sx}^*(\epsilon\eta^*), \tag{7}$$

$$-\epsilon\sigma\tau_{yx}^* \frac{\partial \eta^*}{\partial x^*} - \epsilon\sigma\tau_{yy}^* \frac{\partial \eta^*}{\partial y^*} + \tau_{yz}^* = \tau_{sy}^*(\epsilon\eta^*), \tag{8}$$

$$P^* + \epsilon\sigma\tau_{zx}^* \frac{\partial \eta^*}{\partial x^*} + \epsilon\sigma\tau_{zy}^* \frac{\partial \eta^*}{\partial y^*} - \tau_{zz}^* = 0, \tag{9}$$

at the *bottom*, $z^* = -1 + \sigma^2\xi^*(x^*, y^*, t^*)$

$$\frac{\sigma^2}{\epsilon}\frac{\partial \xi^*}{\partial t^*} + \sigma^2 U^* \frac{\partial \xi^*}{\partial x^*} + \sigma^2 V^* \frac{\partial \xi^*}{\partial y^*} = W^*, \tag{10}$$

$$-\sigma^3\tau_{xx}^* \frac{\partial \xi^*}{\partial x^*} - \sigma^3\tau_{xy}^* \frac{\partial \xi^*}{\partial y^*} + \tau_{xz}^* = \tau_{fx}^*(-1 + \sigma^2\xi^*), \tag{11}$$

$$-\sigma^3\tau_{yx}^* \frac{\partial \xi^*}{\partial x^*} - \sigma^3\tau_{yy}^* \frac{\partial \xi^*}{\partial y^*} + \tau_{yz}^* = \tau_{fy}^*(-1 + \sigma^2\xi^*), \tag{12}$$

By integrating over the water depth the equations (1)–(4), taking into account the boundary conditions (6)–(12), the three-dimensional problem of the horizontal propagation of waves with a current can be reduced to a two-dimensional one. Without other restrictions, the continuity equation is obtained:

$$\frac{\partial}{\partial t^*}(\eta^* - \frac{\sigma^2}{\epsilon}\xi^*) + \frac{\partial}{\partial x^*}[(1 - \sigma^2\xi^* + \epsilon\eta^*)U^*] + \frac{\partial}{\partial y^*}[(1 - \sigma^2\xi^* + \epsilon\eta^*)V^*] = 0. \tag{13}$$

Accepting the basic assumptions of the Boussinesq equations:

$$\sigma^2 \ll 1, \quad U_r = \epsilon/\sigma^2 \approx 1, \quad \Omega_x^* = O(\sigma^4) \text{ and } \Omega_y^* = O(\sigma^4),$$

where U_r is the Ursell number, the integration of the fundamental momentum equations (2) and (3) leads to the following system:

$$\begin{aligned}
&\frac{\partial U^*}{\partial t^*} + \epsilon U^* \frac{\partial U^*}{\partial x^*} + \epsilon V^* \frac{\partial U^*}{\partial y^*} + \frac{\partial \eta^*}{\partial x^*} - \sigma^2 \frac{(1-\sigma^2\xi^*)^2}{3}\left(\frac{\partial^3 U^*}{\partial x^{*2}\partial t^*} + \frac{\partial^3 V^*}{\partial x^*\partial y^*\partial t^*}\right) \\
&-\sigma^3 \frac{(1-\sigma^2\xi^*)^2}{3}\frac{\partial}{\partial x^*}\left[u_c^*\left(\frac{\partial^2 U^*}{\partial x^{*2}} + \frac{\partial^2 V^*}{\partial x^*\partial y^*}\right) + v_c^*\left(\frac{\partial^2 U^*}{\partial x^*\partial y^*} + \frac{\partial^2 V^*}{\partial y^{*2}}\right)\right] \\
&+\frac{\sigma^5}{\epsilon}(1 - \sigma^2\xi^*)\frac{\partial}{\partial x^*}\left(\frac{1}{2\sigma}\frac{\partial^2 \xi^*}{\partial t^{*2}} + u_c^* \frac{\partial^2 \xi^*}{\partial x^*\partial t^*} + v_c^* \frac{\partial^2 \xi^*}{\partial y^*\partial t^*}\right) \\
&-\frac{\sigma}{R}\left(\frac{\partial^2 U^*}{\partial x^{*2}} + \frac{\partial^2 U^*}{\partial y^{*2}}\right) - \frac{\tau_{s_x}^*(\epsilon\eta^*) - \tau_{b_x}^*(-1 + \sigma^2\xi^*)}{\epsilon\sigma(1 - \sigma^2\xi^* + \epsilon\eta^*)} = O(\epsilon^2, \epsilon\sigma^2, \sigma^4, \sigma^2/R),
\end{aligned} \tag{14}$$

$$\frac{\partial V^*}{\partial t^*} + \epsilon U^* \frac{\partial V^*}{\partial x^*} + \epsilon V^* \frac{\partial V^*}{\partial y^*} + \frac{\partial \eta^*}{\partial y^*} - \sigma^2 \frac{(1-\sigma^2\xi^*)}{3}\left(\frac{\partial^3 U^*}{\partial x^* \partial y^* \partial t^*} + \frac{\partial^3 V^*}{\partial y^{*2} \partial t^*}\right)$$

$$-\sigma^3 \frac{(1-\sigma^2\xi^*)^2}{3} \frac{\partial}{\partial y^*}\left[u_c^*\left(\frac{\partial^2 U^*}{\partial x^{*2}} + \frac{\partial^2 V^*}{\partial x^* \partial y^*}\right) + v_c^*\left(\frac{\partial^2 U^*}{\partial x^* \partial y^*} + \frac{\partial^2 V^*}{\partial y^{*2}}\right)\right]$$

$$+\frac{\sigma^5}{\epsilon}(1-\sigma^2\xi^*)\frac{\partial}{\partial y^*}\left(\frac{1}{2\sigma}\frac{\partial^2 \xi^*}{\partial t^{*2}} + u_c^* \frac{\partial^2 \xi^*}{\partial x^* \partial t^*} + v_c^* \frac{\partial^2 \xi^*}{\partial y^* \partial t^*}\right)$$

$$-\frac{\sigma}{R}\left(\frac{\partial^2 V^*}{\partial x^{*2}} + \frac{\partial^2 V^*}{\partial y^{*2}}\right) - \frac{\tau_{s_y}^*(\epsilon\eta^*) - \tau_{b_y}^*(-1+\sigma^2\xi^*)}{\epsilon\sigma(1-\sigma^2\xi^* + \epsilon\eta^*)} = O(\epsilon^2, \epsilon\sigma^2, \sigma^4, \sigma^2/R), \tag{15}$$

where $R = Hc_0/\nu$ is the Reynolds number, ν being the kinematic viscosity; $\tau_b^*(-1+\sigma^2\xi^*)$ and $\tau_s^*(\epsilon\eta^*)$ represents non-dimensional stresses per unit mass, at the bottom and at the surface respectively.

Although mathematically irrelevant at this order of approximation, some terms involving the bottom variable ξ were left, since they were found to be important for the simulations over irregular bathymetries.

In dimensional variables, a complete set of modified Boussinesq equations, here extended in order to take these factors into account: (i) a time-dependent bathymetry; (ii) the friction at the bottom; (iii) a steady current; and (iv) breaking wave conditions, may be written as follows:

$$\frac{\partial h}{\partial t} + \frac{\partial (hU)}{\partial x} + \frac{\partial (hV)}{\partial y} = 0, \tag{16}$$

$$\frac{\partial U}{\partial t} + U\frac{\partial U}{\partial x} + V\frac{\partial U}{\partial y} + g\frac{\partial \eta}{\partial x} - \frac{(H-\xi)^2}{3}\left(\frac{\partial^3 U}{\partial x^2 \partial t} + \frac{\partial^3 V}{\partial x \partial y \partial t}\right)$$

$$-\frac{(H-\xi)^2}{3}\frac{\partial}{\partial x}\left[u_c\left(\frac{\partial^2 U}{\partial x^2} + \frac{\partial^2 V}{\partial x \partial y}\right) + v_c\left(\frac{\partial^2 U}{\partial x \partial y} + \frac{\partial^2 V}{\partial y^2}\right)\right]$$

$$+(H-\xi)\frac{\partial}{\partial x}\left(\frac{1}{2}\frac{\partial^2 \xi}{\partial t^2} + u_c\frac{\partial^2 \xi}{\partial x \partial t} + v_c \frac{\partial^2 \xi}{\partial y \partial t}\right)$$

$$-\nu\left(\frac{\partial^2 U}{\partial x^2} + \frac{\partial^2 U}{\partial y^2}\right) - \frac{\tau_{s_x}(\eta)}{h} + \frac{\tau_{b_x}(\xi)}{h} = 0, \tag{17}$$

$$\frac{\partial V}{\partial t} + U\frac{\partial V}{\partial x} + V\frac{\partial V}{\partial y} + g\frac{\partial \eta}{\partial y} - \frac{(H-\xi)^2}{3}\left(\frac{\partial^3 U}{\partial x \partial y \partial t} + \frac{\partial^3 V}{\partial y^2 \partial t}\right)$$

$$-\frac{(H-\xi)^2}{3}\frac{\partial}{\partial y}\left[u_c\left(\frac{\partial^2 U}{\partial x_2} + \frac{\partial^2 V}{\partial x \partial y}\right) + v_c\left(\frac{\partial^2 U}{\partial x \partial y} + \frac{\partial^2 V}{\partial y^2}\right)\right]$$

$$+(H-\xi)\frac{\partial}{\partial y}\left(\frac{1}{2}\frac{\partial^2 \xi}{\partial t^2} + u_c\frac{\partial^2 \xi}{\partial x \partial t} + v_c \frac{\partial^2 \xi}{\partial y \partial t}\right)$$

$$-\nu\left(\frac{\partial^2 V}{\partial x^2} + \frac{\partial^2 V}{\partial y^2}\right) - \frac{\tau_{s_y}(\eta)}{h} + \frac{\tau_{b_y}(\xi)}{h} = 0, \tag{18}$$

where $h = H - \xi + \eta$.

2.1. Bottom shear stress parametrization

A general expression for the $\tau_b(\xi)/h$ term may be written as an integral approach due to both the current (u_c, v_c) and the waves (u, v):

$$\frac{\vec{\tau}_b(\xi)}{h} = \frac{1}{2h} f_{cw} |\mathrm{V}| \vec{\mathrm{V}}, \tag{19}$$

where $|\mathrm{V}| = \sqrt{(U^2 + V^2)}$ and $\vec{\mathrm{V}} = (U, V)$.

For the wave-current friction factor f_{cw}, in Tolman[11] reference is made to the following approach suggested by Jonsson:

$$f_{cw} = \frac{f_w + \theta f_c}{1 + \theta}; \theta = \frac{|\mathrm{V}_c|}{\hat{\mathrm{V}}_w} \tag{20}$$

in which f_w is determined ignoring the current and f_c is determined ignoring the waves; $\hat{\mathrm{V}}_w$ represents the maximum orbital velocity of the wave.

As we look for a time dependent definition of the friction factor f_{cw}, to be used in any conditions of wave, current and wave-current interaction, the following new local expression for the parameter θ is proposed,

$$\theta = |\mathrm{V}_c|/|\mathrm{V}_w|$$

which leads to:

$$f_{cw} = \frac{|\mathrm{V}_w|}{|\mathrm{V}_w| + |\mathrm{V}_c|} f_w + \frac{|\mathrm{V}_c|}{|\mathrm{V}_w| + |\mathrm{V}_c|} f_c, \tag{21}$$

where $|\mathrm{V}_w| = \sqrt{(u^2 + v^2)}$ and $|\mathrm{V}_c| = \sqrt{(u_c^2 + v_c^2)}$.

In expression (21), both friction factors (f_w and f_c) must incorporate wave and current influences. With an improvement of the factor f_w given by Temperville and Thanh[10] for the wave only,, and the factor f_c given by Van Rijn,[9] the final form of these friction factors is:

$$f_w = 0{\cdot}00278 \exp\left[4{\cdot}65 \frac{|\mathrm{V}_w|}{|\mathrm{V}_w| + |\mathrm{V}_c|} \Phi\left(\frac{\hat{a}}{k_N}\right)^A\right],$$

$$f_c = 0{\cdot}06\left[\log_{10}\frac{12h}{k_{rcw}}\right]^{-2},$$

where Φ depends on the angle ϕ_{wc} between the current and the direction of the wave propagation (with $\phi_{wc} = 0$, $\Phi = 1{\cdot}0$); $A \approx -0{\cdot}22$; $\hat{a} = |\mathrm{V}_w| T/2\pi$, with $\hat{a} \geqslant k_N$; $k_N \approx 2{\cdot}5 d_{50}$ is the equivalent Nikuradse rugosity and $k_{rcw} \approx 3d_{90} \exp[|\mathrm{V}_w|\phi/(|\mathrm{V}_w| + |\mathrm{V}_c|)]$ is a current-related bed-roughness coefficient.

2.2. Parametrization of the wave breaking process

Considering a set of time-dependent mild-slope equations and assuming purely progressive long waves over a uniformly sloping beach, with a constant ratio of wave height to water depth. Watanabe and Dibajnia[12] deduced the following expression for the surface stress per unit mass:

$$\vec{\tau}_s(\eta)/h = f_D \vec{\mathrm{V}},$$

with

$$f_D = \alpha_D \tan\beta \sqrt{(g/h)},$$

where $\tan\beta$ is a representative bottom slope around the breaking point and $\alpha_D \approx 2{\cdot}5$. They also deduced an expression for a general bottom topography, which allows us to compute wave decay and recovery after breaking, but does not take into account the momentum exchange due to turbulence.

Based on this pioneering work, we suggest a formulation given by:

$$\frac{\vec{\tau}_s(\eta)}{h} = -\vec{\nu}_T\left(\frac{\partial^2 \vec{V}}{\partial x^2} + \frac{\partial^2 \vec{V}}{\partial y^2}\right), \tag{22}$$

with the local $\vec{\nu}_T$ components approximated by:

$$(\nu_T)_x = \alpha_B\left(\frac{\partial \xi}{\partial x}\right)_B h\sqrt{gh\frac{V_R}{V_B}}, \tag{23}$$

$$(\nu_T)_y = \alpha_B\left(\frac{\partial \xi}{\partial y}\right)_B h\sqrt{gh\frac{V_R}{V_B}}, \tag{24}$$

being

$$V_B = \Gamma\sqrt{(g/h)}\eta_B, \quad V_R = |V_w| - V_B,$$

or by

$$(\nu_T)_x = 0, \quad \text{if } V_R \leqslant 0 \text{ or } V_B \leqslant (V_f)_x,$$
$$(\nu_T)_y = 0, \quad \text{if } V_R \leqslant 0 \text{ or } V_B \leqslant (V_f)_y,$$

with

$$\vec{V}_f = \Gamma\sqrt{[g(H-\xi)]}\left[\left(\gamma_1 + \gamma_2\frac{\partial \xi}{\partial x}\right)\hat{i} + \left(\gamma_1 + \gamma_2\frac{\partial \xi}{\partial y}\right)\hat{j}\right].$$

V_B represents a critical velocity amplitude for the wave breaking process; $\vec{V}_f$ represents the 'stable' velocity of the wave after each breaking process. $\alpha_B \leqslant 7{\cdot}5$; $\Gamma \approx 0{\cdot}40$; $\gamma_1 \approx 0{\cdot}25$ and $\gamma_2 \geqslant 1{\cdot}0$ are empirical coefficients. The subscript B indicates value at the breaking point.

3. NUMERICAL METHOD

To obtain a numerical solution of the equation system (16)–(18), the finite element method for spatial discretization of the partial differential equations is applied.

3.1. Numerical procedure

Following Antunes do Carmo *et al.*,[2] the (U, V) derivatives in time and third spatial derivatives are grouped in two equations; this means that an equivalent system of five equations is solved instead of the original (16)–(18). Considering a time invariable bathymetry, the final equation system up to the order σ^3 takes the following form:

$$\frac{\partial h}{\partial t} + h\frac{\partial U}{\partial x} + U\frac{\partial h}{\partial x} + h\frac{\partial V}{\partial y} + V\frac{\partial h}{\partial y} = 0, \tag{25}$$

$$\begin{aligned}\frac{\partial r}{\partial t} + u_c\frac{\partial r}{\partial x} + v_c\frac{\partial r}{\partial y} &= (u_c - U)\frac{\partial U}{\partial x} + (v_c - V)\frac{\partial U}{\partial y} - g\frac{\partial(h+\xi)}{\partial x}\\ &+ \frac{(H-\xi)^2}{3}\left[\frac{\partial u_c}{\partial x}\left(\frac{\partial^2 U}{\partial x^2} + \frac{\partial^2 U}{\partial y^2}\right) + \frac{\partial v_c}{\partial x}\left(\frac{\partial^2 V}{\partial x^2} + \frac{\partial^2 V}{\partial y^2}\right)\right]\\ &+ \nu\left(\frac{\partial^2 U}{\partial x^2} + \frac{\partial^2 U}{\partial y^2}\right) + \frac{\tau_{s_x}(\eta)}{h} - \frac{\tau_{b_x}(\xi)}{h},\end{aligned} \tag{26}$$

$$\frac{\partial s}{\partial t}+u_c\frac{\partial s}{\partial x}+v_c\frac{\partial s}{\partial y}=\left(u_c-U\right)\frac{\partial V}{\partial x}+\left(v_c-V\right)\frac{\partial V}{\partial y}-g\frac{\partial(h+\xi)}{\partial y}$$
$$+\frac{(H-\xi)^2}{3}\left[\frac{\partial u_c}{\partial y}\left(\frac{\partial^2 U}{\partial x^2}+\frac{\partial^2 U}{\partial y^2}\right)+\frac{\partial v_c}{\partial y}\left(\frac{\partial^2 V}{\partial x^2}+\frac{\partial^2 V}{\partial y^2}\right)\right]$$
$$+\nu\left(\frac{\partial^2 U}{\partial x^2}+\frac{\partial^2 V}{\partial y^2}\right)+\frac{\tau_{s_y}(\eta)}{h}-\frac{\tau_{b_y}(\xi)}{h}, \tag{27}$$

$$U-\frac{(H-\xi)^2}{3}\left(\frac{\partial^2 U}{\partial x^2}+\frac{\partial^2 U}{\partial y^2}\right)=r, \tag{28}$$

$$V-\frac{(H-\xi)^2}{3}\left(\frac{\partial^2 V}{\partial x^2}+\frac{\partial^2 V}{\partial y^2}\right)=s. \tag{29}$$

We also assumed that $\Omega_z^* = O(\sigma^2)$, which strictly corresponds to a limitation of the numerical method to weakly vertical rotational flows. However, as we will see later, even in severe conditions (e.g. behind obstacles) the model seems to behave well. This assumption is not essential for the development of the method and it is used here in order to reduce the computational effort.

As the values of variables h, U, V, r and s are known at time t, we can use a numerical procedure based on the following steps (with $\theta \approx 0{\cdot}5$) to compute the corresponding values at time $t+\Delta t$.

1. The equation (25) allows us to predict the values of variable $h(h_p^{t+\Delta t})$, considering the known values of h, U and V at time t in the whole domain.
2. Equations (26) and (27) make it possible to predict the values of variables $r(r_p^{t+\Delta t})$ and $s(r_p^{t+\Delta t})$, taking into account the values of U^t, V^t, r^t, s^t and $\tilde{h}^{t+\theta\Delta t} = (1-\theta)h^t + \theta h_p^{t+\Delta t}$, known for the whole domain.
3. Solutions of equations (28) and (29) give us the values of the mean-averaged velocity components U and V ($U^{t+\Delta t}$ and $V^{t+\Delta t}$), taking into account the predicted values of r and $s(r_p^{t+\Delta t}$ and $s_p^{t+\Delta t}$ respectively).
4. Equation (25) allows us to compute the depth h at time $t+\Delta t$ (values of $h^{t+\Delta t}$), considering the values of variables h^t, $U^{t+\theta\Delta t} = (1-\theta)U^t + \theta U^{t+\Delta t}$ and $V^{t+\theta\Delta t} = (1-\theta)V^t + \theta V^{t+\Delta t}$ known for the whole domain.
5. Equations (26) and (27) allows us to compute the values of variables r and s at time $t+\Delta t$ (values of $r^{t+\Delta t}$ and $s^{t+\Delta t}$), taking into account the values $r^t, s^t, h^{t+\theta\Delta t} = (1-\theta)h^t + \theta h^{t+\Delta t}$, $U^{t+\theta\Delta t} = (1-\theta)U^t + \theta U^{t+\Delta t}$ and $V^{t+\theta\Delta t} = (1-\theta)V^t + \theta V^{t+\Delta t}$ known for the whole domain.

Similar schemes can be found in Seabra-Santos *et al.*[3] and Abreu and Seabra-Santos.[1]

3.2. *Development of the method*

If Δ^e is a generic element, considering the generic function p (here representing any of the variables h, U, V, r or s, and yet u_c, v_c and ξ or $(H-\xi)$ approximated within each element by:

$$p \approx \hat{p} = \sum_{i=1}^{n} N_i p_i, \tag{30}$$

where p_i is the value of the function p at the node i of the element Δ^e, n is the number of nodes of the element and N_i is the interpolation (shape) function N corresponding to the i-node of the element Δ^e.

As the assumed functional form of the variables (generic $\hat{p}$) are only approximate, the substitution of $\hat{p}$ in any equation (J) (J varying between 25 to 29) generates a residual R_J. According to the weighted residual technique, minimization requires the 'orthogonality' of the residual R_J to a set of weighting functions W_i, i.e.

$$\int_{\Delta^e} W_i R_J \, \mathrm{d}\Delta^e = 0. \tag{31}$$

Different forms of the weighting functions may be utilized. For instance, the Petrov-Galerkin procedure is here utilized to achieve solutions for the unknowns h, r and s (equations (25)–(27)). The general form of the weighting functions applied to these equations is defined as

$$W_i = N_i + \beta_{u_i}\frac{\partial N_i}{\partial x} + \beta_{v_i}\frac{\partial N_i}{\partial y}, \quad i = 1, \cdots, n, \tag{32}$$

where the β_{u_i} and β_{v_i} coefficients are functions of: (i) the local velocities U and V; (ii) the ratio of the wave amplitude to the water depth; and (iii) the element length.

With $W_i = N_i$ another weighted residual technique is obtained, known as the Galerkin procedure. Solutions for the unknowns U and V (equations (28) and (29)) are achieved through minimisation of their residuals (residuals R_{28} and R_{29}, respectively) utilizing this technique.

To illustrate this procedure, a complete solution of equation (28) is presented here in detail.

Introducing in equation (28) the approximated values given by (30), the following residual R_{28} is obtained:

$$R_{28} = \hat{U} - \frac{\widehat{(H-\xi)^2}}{3}\left(\frac{\partial^2 \hat{U}}{\partial x^2} + \frac{\partial^2 \hat{u}}{\partial y^2}\right) - \hat{r}. \tag{33}$$

According to Galerkin's procedure, after using integration by parts (or Green's theorem) to reduce the second derivatives, the R_{28} error minimization leads to the following equation (up to the order σ^3):

$$\begin{aligned}\int_{\Delta^e} & N_i R_{28} \, \mathrm{d}\Delta^e \\ &= \int_{\Delta^e}\left\{N_i \sum_{j=1}^{n} N_j U_j + \sum_{k=1}^{n} N_k \frac{(H-\xi)_k^2}{3}\left[\frac{\partial N_i}{\partial x}\sum_{j=1}^{n}\frac{\partial N_j}{\partial x} + \frac{\partial N_i}{\partial y}\sum_{j=1}^{n}\frac{\partial N_j}{\partial y}\right]U_j - N_i \sum_{j=1}^{n} N_j r_j\right\} \mathrm{d}\Delta^e \\ &\quad - \oint_{\Gamma^e} N_k \frac{(H-\xi)_k^2}{3} N_i \frac{\partial N_j}{\partial n} U_j \, \mathrm{d}\Gamma^e.\end{aligned} \tag{34}$$

The boundary integral presented in the right-hand side of equation (34) may be subdivided into two parts:

$$\oint_{\Gamma^e} N_k \frac{(H-\xi)_k^2}{3} N_i \frac{\partial N_j}{\partial n} U_j \, \mathrm{d}\Gamma^e = \oint_{\Gamma_i^e} N_p \frac{(H-\xi)_p^2}{3} N_q \frac{\partial N_r}{\partial n} U_r \, \mathrm{d}\Gamma_i^e + \oint_{\Gamma_e^e} N_p \frac{(H-\xi)_p^2}{3} N_q \left(\frac{\partial U}{\partial n}\right) \mathrm{d}\Gamma_e^e,$$

where Γ_i^e represents the element sides within the domain, with the corresponding integral null because the resulting element contributions are equal, but with opposite signals, and Γ_e^e represents the element sides coincident with the boundary domain.

Accordingly, an equivalent form of equation (34), taking into account (31), may be written as follows:

$$\int_{\Delta^e}\left\{N_i\sum_{j=1}^{n}N_j+\sum_{k=1}^{n}N_k\frac{(H-\xi)_k^2}{3}\left[\frac{\partial N_i}{\partial x}\sum_{j=1}^{n}\frac{\partial N_j}{\partial x}+\frac{\partial N_i}{\partial y}\sum_{j=1}^{n}\frac{\partial N_j}{\partial y}\right]\right\}U_j\,\mathrm{d}\Delta^e$$
$$=\int_{\Delta^e}N_i\sum_{j=1}^{n}N_jr_j\,\mathrm{d}\Delta^e+\oint_{\Gamma_e^e}N_p\frac{(H-\xi)_p^2}{3}N_q\left(\frac{\partial U}{\partial n}\right)\mathrm{d}\Gamma_e^e, \tag{35}$$

with $p,\ q=1,\dots,n_e$, where n_e is the number of nodes of the corresponding element side coincident with the boundary domain.

These equations may be written in matrix form as follows:

$$[A]\{U\}=\{B\}, \tag{36}$$

where matrix A and vector B elements are given by

$$a_{i,j}=\int_{\Delta^e}\left\{N_iN_j+\sum_{k=1}^{n}N_k\frac{(H-\xi)_k^2}{3}\left[\frac{\partial N_i}{\partial x}\frac{\partial N_j}{\partial x}+\frac{\partial N_i}{\partial y}\frac{\partial N_j}{\partial y}\right]\right\}\mathrm{d}\Delta^e,$$

$$b_i=\int_{\Delta^e}N_i\sum_{j=1}^{n}N_jr_j\,\mathrm{d}\Delta^e+\oint_{\Gamma_e^e}N_p\frac{(H-\xi)_p^2}{3}N_q\left(\frac{\partial U}{\partial n}\right)\mathrm{d}\Gamma_e^e,$$

$i,j=1,\dots,n$ and $p,q=1,\dots,n_e$.

A suitable grid is normally crucial to the success of a finite element model. In our case, the following rules must be fulfilled for its generation.

(*a*) Element side lower than the local depth.
(*b*) Minimum of 20 to 25 elements per wave length.
(*c*) Courant number always lower than one in the whole domain.

Several regular and highly irregular quadrilateral grids that fulfilled the above-mentioned rules have been used up to the present and the model seems to behave well in all tested cases.

3.3. Boundary conditions

Equations (28) and (29) are of the elliptic type, so imposition of natural and/or essential boundary conditions is necessary in all boundary nodes of the domain.

Natural boundary conditions for the U and/or V variables (known values of the $\partial U/\partial n$ and/or $\partial V/\partial n$ quantities) are introduced from the boundary integral presented in the B vector of equation system (36) and/or equivalent for equation (29).

The essential boundary conditions of the type $p=p_b$ may be introduced in the final system (equation system (36) for the U variable and/or equivalent for V), after adding up the contributions from all elements and all sides with natural boundary conditions (values of $\partial p/\partial n\neq 0$), by eliminating the rows corresponding to the prescribed unknowns and inserting the contributions of those prescribed unknowns on the right-hand side.

On the incident side boundary, the waves are expressed as the superposition of the incident wave (any complex signal) and the outgoing wave.

Considering an incident wave in the x-direction, for the problems discussed here this condition takes the following form

$$U=u_c\left(1-\frac{\eta}{h}\right)+\mathrm{v_I}+(\mathrm{v_I}-\mathrm{v_O})|\cos\alpha|, \tag{37}$$

where $\vee_I$ represents the velocity of the incident wave (sinusoidal, cnoidal, solitary, irregular), and the angle α is the outgoing wave direction measured from the x-axis. The outgoing component of the wave $\vee_O$ is expressed as

$$\vee_O = \sqrt{\frac{g}{h}}\,\eta, \tag{38}$$

where η is the predicted surface elevation.

On the opposite open boundary (onshore boundary normal to x-axis), the wave velocity is calculated by

$$U = u_c(1 + \eta/h) + \vee_O|\cos\alpha|. \tag{39}$$

In both open boundary cases, a zero natural boundary condition for the V-component of the flow velocity is considered here, i.e.

$$\partial V/\partial n = 0. \tag{40}$$

For a total reflective boundary, if an angle β is defined as the angle formed between the x-axis and the boundary normal, we have the following relation between U and V:

$$U\cos\beta + V\sin\beta = 0. \tag{41}$$

4. EXPERIMENTAL VERSUS COMPUTATIONAL TESTS

Several sets of experiments have been performed by the authors in the Laboratory of Hydraulics of the University of Coimbra, in order to test the mathematical model, as well as numerical results of wave-current interactions, breaking waves over a slope and other characteristic properties of shallow-water, like shoaling, reflexion and diffraction.

In the next sections we will briefly present three of these experiments.

4.1. Wave–current interactions

Within a 4 m long and 0·6 m wide channel, a surface flow is established with 6·9 cm depth and a mean horizontal velocity of 8·5 cm/s.

A plunging piston situated at the upstream region centred at $x = 0{\cdot}45$ m generates a 1 s wave period. At each end of the channel, two wave absorbers virtually guarantee non-reflected waves. Five surface gauges are located at different positions. The signal of the gauge situated at $x = 1{\cdot}1$ m gives the input boundary condition for running the numerical model.

A classical pattern for shallow water non-linear waves ($A/H \approx 0{\cdot}3$) may be seen (Figure 1), where decomposition takes place and the resulting wave train interacts with the current. The agreement between the two results may be considered generally good, for both wave amplitude and phase.

However, it is important to note that the computed and measured results at the signal gauge present slight differences. These can be explained as follows: (i) the incident boundary condition is expressed as the linear superposition of the measured current and approximated wave velocity calculated by an equation similar to (38), in which h and η are the measured quantities. However, the computed free-surface elevations represent the final non-linear response of the model at each time step; (ii) in all numerical computations we assumed totally non-reflective incident and opposite boundaries. In reality, this is not absolutely true and the free-surface elevations at these boundaries are consequently overpredicted.

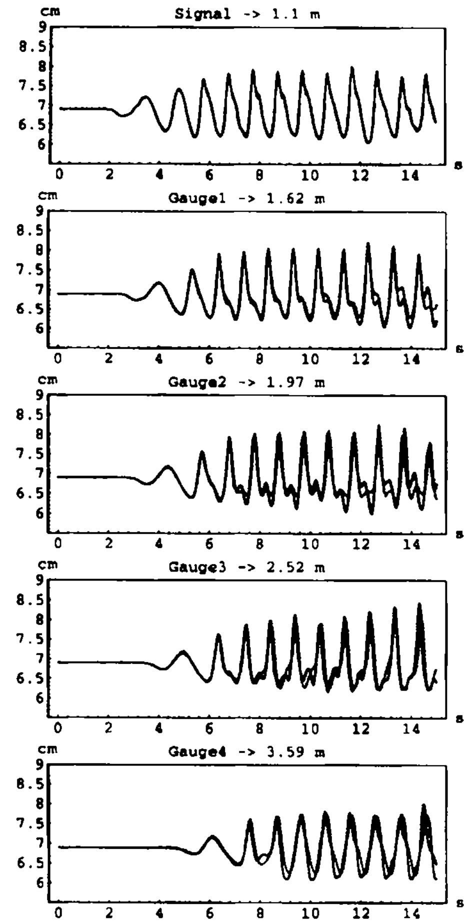

Figure 1. Free surface elevations with time for wave–current interactions: waves propagating with the current. $H_0 = 6{\cdot}9$ cm; $T = 1$ s; $u_c = 8{\cdot}5$ cm/s. ———, Experimental data; - - - - - -, numerical results

Results from another experiment are presented in Figure 2, with the wave generator situated now at the downstream region centred at $x = 3{\cdot}7$ m. A 1 s wave period is propagating against a 6 cm/s current over a 6·6 cm depth. The gauge located at $x = 3{\cdot}2$ m gives the input signal for running the numerical model.

Important non-linear effects are also present in this experiment ($A/H \approx 0{\cdot}26$). A slight loss in phase accuracy and wave height is shown; however, the results may be considered globally good.

4.2. Breaking waves over a slope

Here we consider the propagation and breaking of a wave over a varying depth rigid beach in a 7·5 m long by 0·3 m wide rectangular channel.

The bottom is formed by two horizontal platforms of 1·13 and 1·60 m length, with elevations of 0 m and 0·2 m respectively, located at each end of the channel (0 m $< x \leqslant 1{\cdot}13$ m and 5.40 m $< x \leqslant 7$ m) and joined by a slope of 4·27 m length ($1{\cdot}13$ m $< x \leqslant 5{\cdot}40$ m). The upstream undisturbed depth is 24·9 cm.

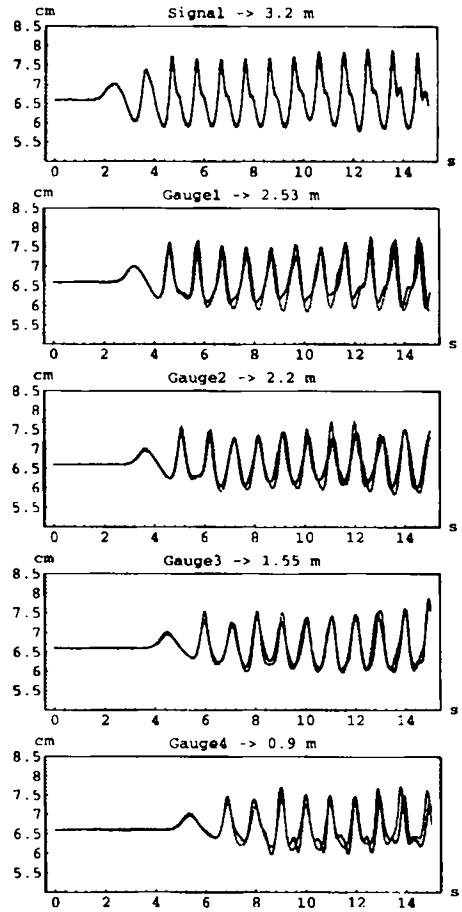

Figure 2. Free surface elevations with time for wave–current interactions: waves propagating against the current. $H_0 = 6{\cdot}6$ cm; $T = 1$ s; $u_c = -6$ cm/s. ———, Experimental data; - - - - - -, numerical results

A 1·72 s wave period is generated which corresponds to a wavelength of 2·53 m ($kh \approx 0{\cdot}62$, where k is the wavenumber), with an amplitude of 2·2 cm. The signal collected by the first proble ($x = 0$) is used as an input boundary condition for modelling the shoaling, decomposition and breaking of the wave over the slope.

Although the experimental conditions are very severe and theoretically outside the application range of this model (slope of 4·7%, breaking occurring over the downstream horizontal platform between gauge 1 and gauge 3, very high reduced amplitude, intermediate depth water conditions in the upstream region), the results presented in Figure 3 are in good agreement with the experimental data.

It is important to note that the classical Boussinesq wave model, which does not include breaking conditions, gives in this example, e.g. at gauge 3, water elevations up to 29 cm ($A/H \approx 0{\cdot}84$) which represents an error of about 80%, and overestimates decomposition.

4.3. *Wave–current diffraction by a vertical cylinder*

Numerical three-dimensional results are compared with those obtained experimentally in the first facility described above (a 4 m long and 0·6 m wide channel) with the centre of a vertical circular

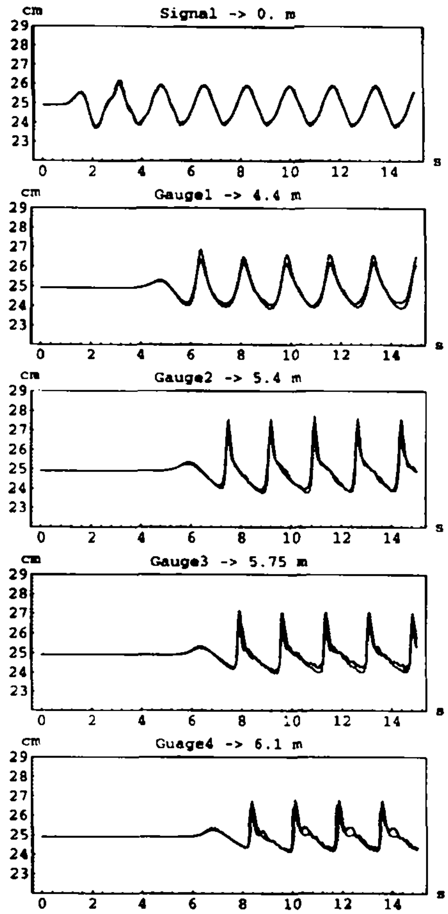

Figure 3. Breaking waves over a slope of 4·7%: free-surface elevations with time from computation and experimental measurement. $H_0 = 24{\cdot}9$ cm; $H_1 = 4{\cdot}9$ cm; $A_0 = 2{\cdot}2$ cm; $T = 1{\cdot}72$ s ($kh \approx 0{\cdot}62$). ————, Experimental data; - - - - - -, numerical results

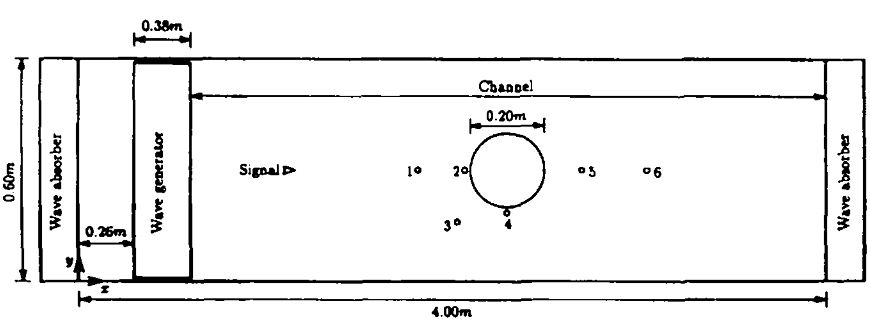

Figure 4. Plan view and installed depth gauges for a wave–current diffraction by a vertical circular cylinder

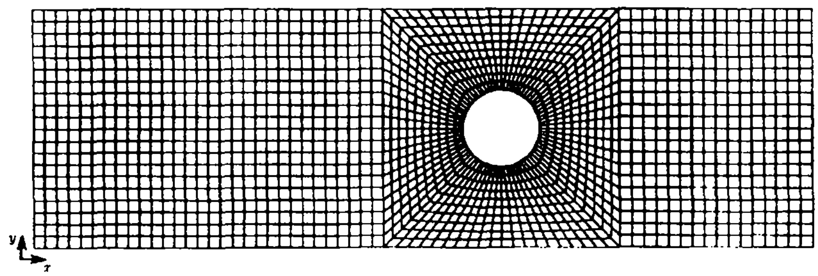

Figure 5. Wave–current diffraction by a vertical cylinder: computational mesh

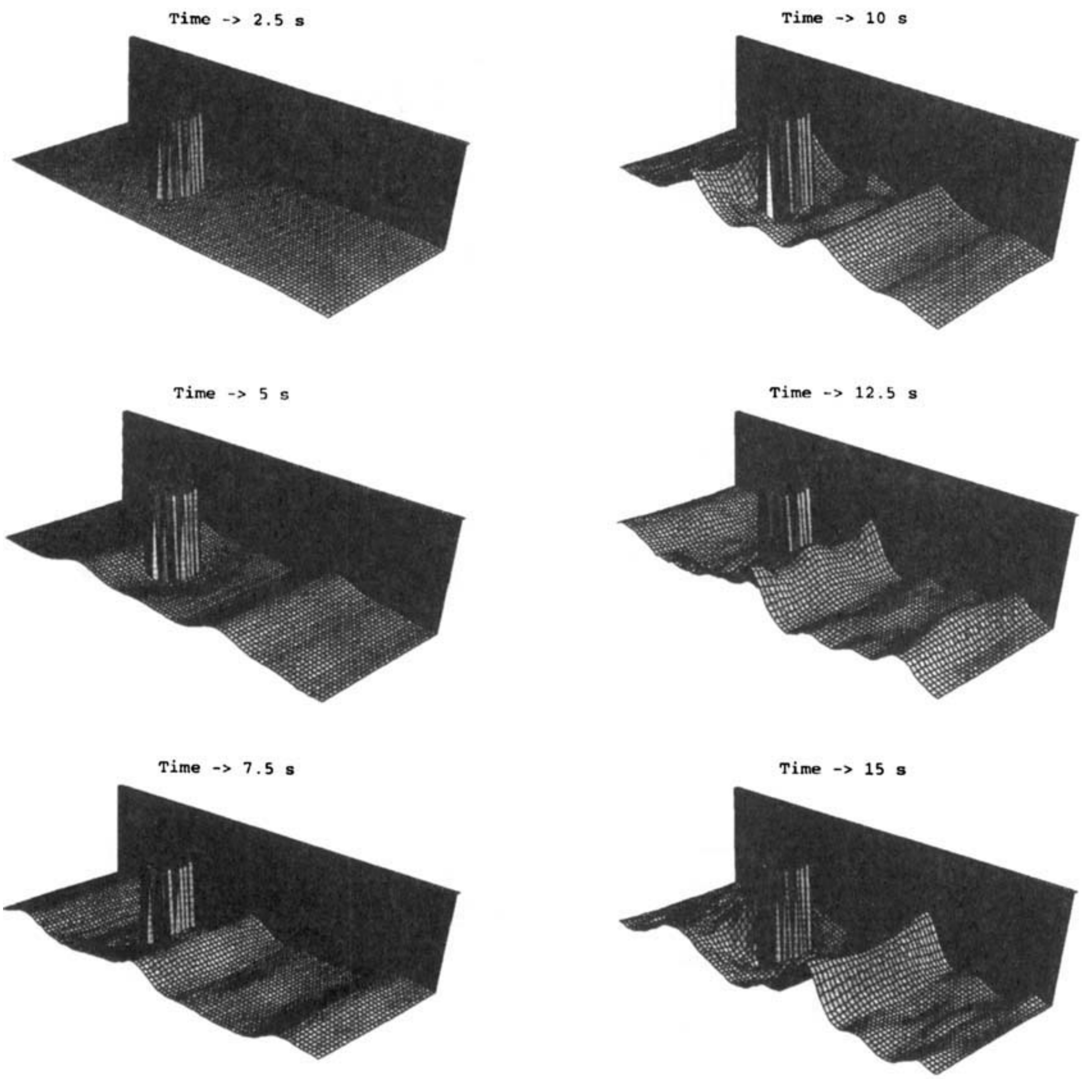

Figure 6. Wave–current diffraction by a vertical cylinder: three-dimensional perspective view of free-surface elevation, in time sequence. The closest wall of the channel was removed for better visualization

cylinder, 20 cm in diameter, located at $x = 2{\cdot}3$ m and $y = 0{\cdot}3$ m. The cylinder pierces the free surface. Seven gauges are located at different positions (Figure 4).

A surface flow is established, for an imposed mean horizontal velocity of 8·5 cm/s at the first section of the channel. At the signal probe ($x = 1{\cdot}1$ m), the mean water depth remains about 7 cm.

A plunging piston centred at $x = 0{\cdot}45$ m generates a 1 s wave period. The probe located at $x = 1{\cdot}1$ m gives the input boundary condition for the numerical model.

The computational mesh used in this simulation is composed by four-node elements. It is presented in Figure 5.

Numerical results are shown in Figure 6, representing the domain at times $t_1 = 2{\cdot}5$ s, $t_2 = 5$ s, $t_3 = 7{\cdot}5$ s, $t_4 = 10$ s, $t_5 = 12{\cdot}5$ s and $t_6 = 15$ s, and where the closest wall of the channel was removed for better visualization.

Figure 7 shows the comparison between the computed and measured results. Good agreement is obtained.

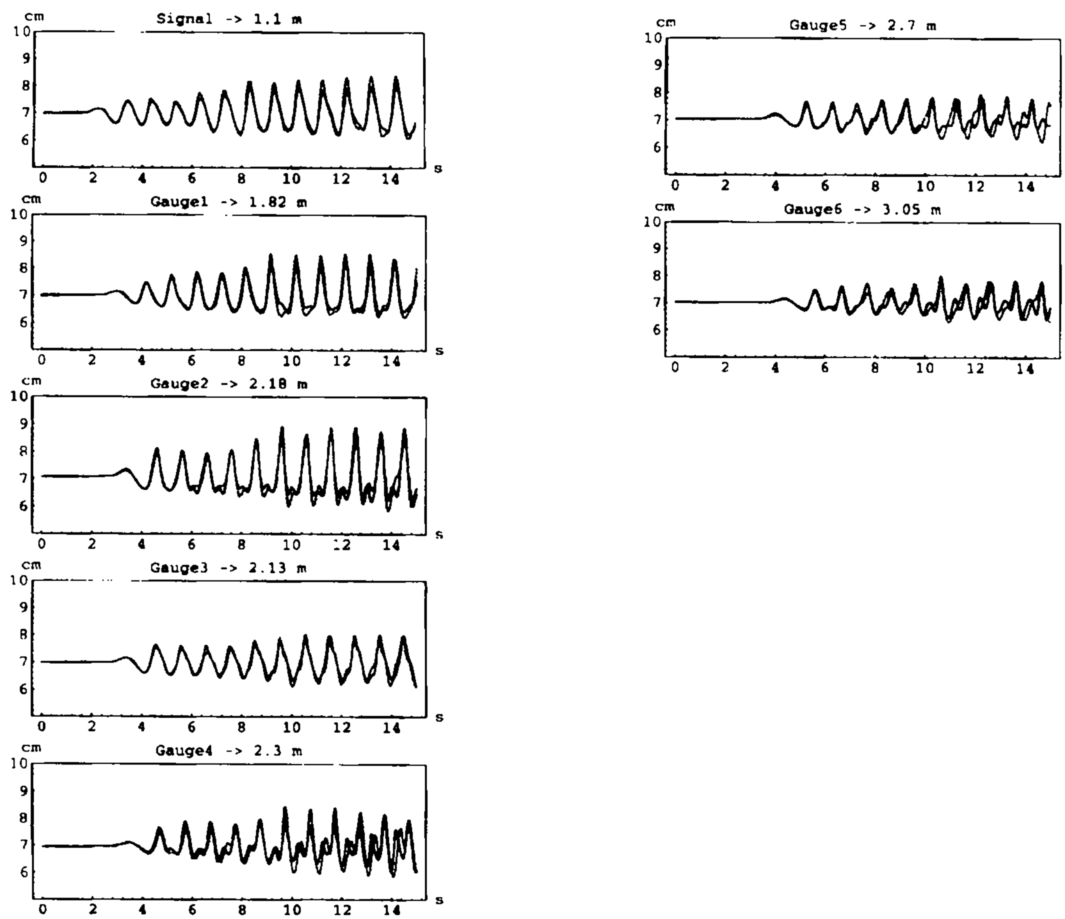

Figure 7. Wave–current diffraction by a vertical cylinder: free-surface elevations with time from computation and experimental measurement. $\bar{H} = 7$ cm; $T = 1$ s; $\bar{u}_c = 8{\cdot}5$ cm/s. Gauges positions in meters: gauge1 (1·82, 0·30), gauge2 (2·18, 0·30), gauge3 (2·13, 0·16), gauge4 (2·30, 0·18), gauge5 (2·70, 0·30), gauge6 (3·05, 0·30). ———, Experimental data; - - - - - -, numerical results

5. CONCLUSIONS

It seems clear from comparisons that the model presented is capable of reproducing the flow characteristics for the proposed examples.

Moreover, its range of application includes intermediate water conditions (values of $kh \leqslant 1{\cdot}0$).

It should be also pointed out that it may be used in any geometry, with an irregular bathymetry, and under complicated boundary conditions, without significant additional computational effort.

Furthermore, as it uses four-node elements, the method is not very costly in time (about 25 s of CPU in a Digital Alpha 3000/500 AXP computer with open VMS AXP v1·5 per time step per 10 000 elements), so a large area of thousands of elements may realistically be treated.

Therefore, we think that it is a valuable tool for studying the surface evolution of coastal and estuarine zones as well as for providing accurate potential flow parameters for further developments concerning the bottom boundary layer and sediment transport.

REFERENCES

1. J. M. Abreu and F. J. Seabra-Santos, 'Generation and propagation of tsunamis produced by the movement of the ocean bed'. *Annales Geophysicae*, **10**, 1–11 (1992).
2. J. S. Antunes do Carmo, F. J. Seabra-Santos, and E. Barthélemy, 'Surface waves propagation in shallow-water: A finite element model'. *Int. j. numer. methods fluids*, **16**, 447–459 (1993).
3. F. J. Seabra-Santos, D. P. Renouard and A. M. Temperville, 'Numerical and experimental study of the transformation of a solitary wave over a shelf or isolated obstacle'. *J. Fluid Mech.*, **176**, 117–134 (1987).
4. W. D. Grant and O. S. Madsen, 'Combined wave and current interaction with a rough bottom'. *J. Geophys. Res.*, **84**, 1797–1808 (1979).
5. I. G. Jonsson, 'Wave-current interactions'. Report No. S 49. The Danish Center for Applied Mathematics and Mechanics. Institute of Hydrodynamics and Hydraulic Engineering, 1989.
6. J. T. Kirby, 'A note on linear surface wave-current interaction over slowly varying topography'. *J. Geophys. Res.*, **89**, 745–747 (1984).
7. M. S. Longuet-Higgins and R. W. Stewart, 'The changes in amplitude of short gravity waves on steady non-uniform currents'. *J. Fluid. Mech.*, **10**, 529–549 (1961).
8. H.-H. Prüser and W. Zielke, 'Irregular waves on a current'. In *Proc. 22nd Int. Coastal Eng. Conf.*, Delft, pp. 1088–1101, 1990.
9. L. C. Van Rijn and A. Kroon, 'Sediment transport by currents and waves'. In *Proc. 23rd Int. Coastal Eng. Conf.*, Venice, pp. 2613–2628, 1992.
10. A. M. Temperville and S. Huynh Thanh, 'Modelisation de la couche limite turbulente oscillatoire generée par l'interaction houle-courant en zone cotière'. Rapport de recherche concernant la modelisation en domaine littoral et cotier, Institut de Mécanique de Grenoble, 1990.
11. H. L. Tolman, 'An evaluation of expressions for wave energy dissipation due to bottom friction in the presence of currents'. *Coastal Engineering*, **16**, 165–179 (1992).
12. A. Watanabe and M. Dibajnia, 'A numerical model of wave deformation in surf zone'. In *Proc. 21st Int. Coastal Eng. Conf.*, Malaga, pp. 578–587, 1988.